Lab on a Chip

Micro- & nano- fluidic research for chemistry, physics, biology, & bioengineering

www.rsc.org/loc

Volume 10 | Number 22 | 21 November 2010 | Pages 2997–3184

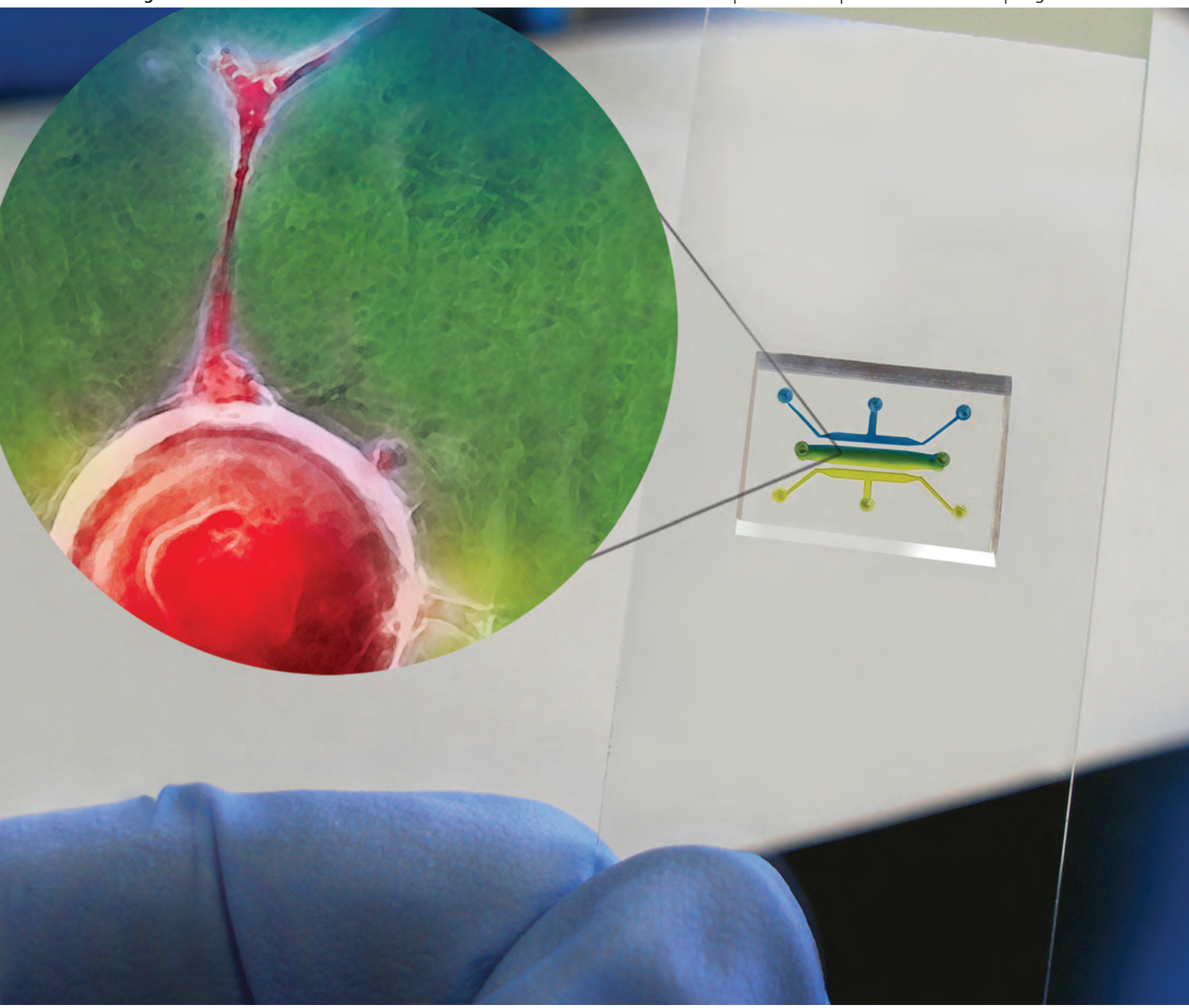

ISSN 1473-0197

RSC Publishing

PAPER

Shamloo and Heilshorn
Matrix density mediates polarization and lumen formation of endothelial sprouts in VEGF gradients

Celebrating 10 Years of publishing

1473-0197(2010)10:22;1-5

Matrix density mediates polarization and lumen formation of endothelial sprouts in VEGF gradients†

Amir Shamloo[a] and Sarah C. Heilshorn*[b]

Received 13th April 2010, Accepted 26th July 2010
DOI: 10.1039/c005069e

Published on 01 September 2010 on http://pubs.rsc.org | doi:10.1039/C005069E
Downloaded by Stanford University on 29/03/2013 22:44:17.

Endothelial cell (EC) sprouting morphogenesis is a critical step during angiogenesis, the formation of new blood vessels from existing conduits. Here, three-dimensional sprouting morphogenesis was examined using *in vitro* microfluidic devices that enabled the separate and simultaneous tuning of biomechanical and soluble biochemical stimuli. Quantitative analysis of endothelial sprout formation demonstrated that the ability of vascular endothelial growth factor (VEGF) to regulate stable sprout formation was mediated by the density of the surrounding collagen/fibronectin matrix. The coordinated migration and proliferation of multiple ECs to form stable sprouts were enhanced at intermediate matrix densities (1.2–1.9 mg ml^{-1}), while lower densities resulted in uncoordinated migration (0.3–0.7 mg ml^{-1}) and higher densities resulted in broad cell clusters that did not elongate (2.7 mg ml^{-1}). Within the permissive range of matrix biomechanics, higher density matrices resulted in shorter, thicker, and slower-growing sprouts. The sprouts in higher density matrices also were more likely to polarize towards higher VEGF concentrations, included more cells per cross-sectional area, and demonstrated more stable lumen formation compared to sprouts in lower density matrices. These results quantitatively demonstrate that matrix density mediates VEGF-induced sprout polarization and lumen formation, potentially by regulating the balance between EC migration rate and proliferation rate.

Introduction

While the biochemical properties of the extracellular matrix (ECM) have long been recognized as playing a critical role in regulating cell behavior, the importance of ECM biomechanics has been highlighted only more recently.[1–4] The mechanical stiffness of ECM has been shown to influence mesenchymal stem cell fate,[5] mammary epithelial cell metastasis,[6] and cell migration.[7] Mechanical forces have also been shown to mediate the migration of single endothelial cells (ECs),[8] pairs of ECs,[9] and the coordinated motion of multiple ECs to form capillary-like sprouts.[10,11] This coordinated EC sprouting morphogenesis is an early stage of angiogenesis, the formation of new blood vessels from existing conduits.

In early angiogenesis stages, ECs migrate from the lumen of developed blood vessels into the surrounding ECM.[12] Through the coordinated actions of migration and proliferation, these ECs organize into tubular capillary-like structures called sprouts.[12] Sprout stabilization occurs through the recruitment of additional cell types and reorganization of the ECM, resulting in maturation of the new vessels.[12] Given the complexity of angiogenesis *in vivo*, several groups have developed controlled *in vitro* platforms to systematically study key steps of the angiogenic process. These assays have included investigations of EC migration and sprouting in response to biomechanical factors in two dimensions (2D)[9] and three dimensions (3D)[10,11,13] as well as application of soluble biochemical factors in 2D[14,15] and 3D.[16,17] However, few *in vitro* platforms have been described that enable simultaneous, quantitative control over both biomechanical and soluble biochemical factors. Here we present the design and fabrication of a device that produces stable growth factor gradients within a 3D matrix to study the interplay of biomechanics and soluble biochemical factors during EC sprouting morphogenesis. Similar to previous gradient generator devices used for 2D cell culture studies, our device utilizes a convective flow barrier to create a stable diffusive gradient across a cell culture chamber.[18–21] The ease of fabrication and concentration gradient generation within this device has made it appropriate for reproducible 3D tissue culture studies. Minimized contact between the matrix and the fluid flow promotes the stability of the matrix for long periods of time. The ease of confocal imaging through a thin layer of the matrix formed within the microfluidic device provides an appropriate condition for detecting delicate 3D tissue features such as lumen formation of endothelial cell sprouts.

In developing our model, we utilized a protocol that enables ECs to undergo a transition from the 2D to 3D culture environment that mimics the physiological process.[11,16,22] *In vivo*, monolayers of ECs initially experience the 2D environment of the luminal surface; however, as they begin sprouting, they are exposed to the 3D environment of the surrounding ECM. It has been widely reported that cell morphology,[23] cell–matrix contacts,[24] signaling cascades,[25] cell migration,[7] and gene expression[25] are different when cells are cultured in 2D versus 3D; therefore, it is critical to develop *in vitro* platforms that mimic the dimensionality of the *in vivo* process. In our system, ECs are initially cultured as 2D monolayers on the surfaces of microcarrier beads. These cell-coated beads are embedded within a collagen/fibronectin matrix of a given density and subjected to

[a]*Mechanical Engineering, Stanford University, Stanford, CA, 94305, USA*
[b]*Materials Science and Engineering, Stanford University, 476 Lomita Mall, McCullough 246, Stanford, CA, 94305-4045, USA. E-mail: Heilshorn@stanford.edu; Fax: +1 650-498-5596; Tel: +1 650-723-3763*

† Electronic supplementary information (ESI) available: Rheology of matrices and sprout formation in uniform VEGF concentrations. See DOI: 10.1039/c005069e

Published on 01 September 2010 on http://pubs.rsc.org | doi:10.1039/C005069E
Downloaded by Stanford University on 29/03/2013 22:44:17.

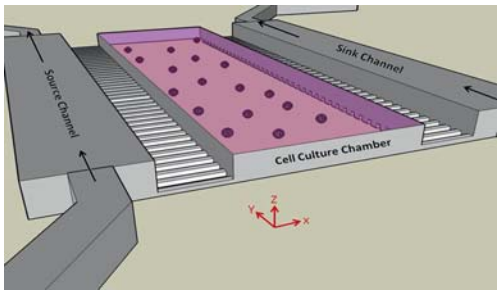

Fig. 1 Schematic of microfluidic system. The device is composed of source and sink channels connected to a cell culture chamber by microcapillaries (20 μm width repeated every 20 μm, not drawn to scale) allowing the formation of a stable concentration gradient. The cell culture chamber ($W \times L \times H$, 1 mm × 4 mm × 240 μm) is loaded with a collagen/fibronectin gel (pink) containing endothelial cell-coated microcarrier beads.

equilibrium VEGF concentration gradients for multiple days inside a microfluidic device (Fig. 1). Upon VEGF stimulation, ECs leave the surfaces of the beads to explore the 3D matrix and potentially undergo sprouting morphogenesis depending on the presence of appropriate biomechanical and biochemical stimuli.

Building on previous reports that EC sprouts alter their morphology within matrices of varying stiffness,[10,13,26] we investigate here the interplay between matrix density and VEGF concentration profiles in guiding EC sprout formation and the stability of their lumen within a 3D matrix. This experimental platform is unique from previously reported devices that permitted EC sprouts to grow along a rigid 2D substrate while covered by a compliant 3D matrix.[27] Our results suggest that matrix density regulates the balance between EC migration rate and proliferation rate, which mediates the kinetics and morphology of VEGF-induced sprouting morphogenesis, polarization, and lumen formation.

Because angiogenesis is a critical process in wound healing,[28] cancer development,[29] tissue engineering,[30] and ischemia treatment;[31] having a deep understanding of the key regulators of this process may lead to the development of new pro- and anti-angiogenic strategies for a variety of applications. For example, the device described here may be a useful screening platform to identify anti-angiogenic pharmaceuticals for cancer therapeutics or to identify biomaterial scaffolds that promote angiogenesis for new regenerative medicine therapies. These reductionist *in vitro* assays may also serve as ideal models to test hypotheses of tumor angiogenesis. For example, it has been observed that blood vessels near tumors are found to show less stable lumen formation with subsequent blood leakage.[32] Coupled with observations that tissue stiffness is modified during tumor progression,[6] these findings suggest that blood vessel stability near and within tumors may respond to both complex VEGF concentration profiles and matrix density variations.

Materials and methods

Microfluidic device fabrication

Soft lithography techniques were used to fabricate the microfluidic devices. Two layers of fluidic channels were designed by AutoCad software and patterned on transparency masks. The Stanford Microfluidics Foundry fabricated a silicon wafer master mold using negative photoresist (SU-8). PDMS (Sylgard 184, Midland, MI) was used to fabricate the microfluidic devices using micromolding against the silicon mold treated with chlorotrimethylsilane (Sigma). Inlets and outlets of the cell culture chamber and the reagent channels were punched using sharpened needles (20 gauge). To adhere the PDMS mold to glass, both surfaces were exposed to oxygen plasma for 2–3 minutes and bound together irreversibly.

Concentration gradient generation

To generate a stable concentration gradient across the cell culture chamber, tubings (Upchurch Scientific, Oak Harbor, WA) were inserted into the inlets of the reagent channels and connected to 100 μl syringes (Hamilton, Reno, NV) mounted on a syringe pump (World Precision Instruments, Sarasota, FL). The injection flow rate was 40 nl min^{-1}. To measure the reagent concentration distribution inside the cell culture chamber, FITC–dextran (M_w = 20 kDa, Sigma) with a similar molecular weight to the protein VEGF-165 (M_w = 20 kDa) was used. This fluorescent biomarker was dissolved in phosphate buffered saline (PBS) and injected into the source channel of the microfluidic device while dextran-free PBS was injected into the sink channel. A fluorescent inverted microscope (Zeiss, Oberkochen, Germany) with a CCD camera was used for imaging. MATLAB software was used to measure the fluorescence intensity of each image pixel inside the cell culture chamber and to normalize against the fluorescence of solutions of known concentrations. This procedure was repeated for each collagen/fibronectin gel density.

Matrix rheology

Rheological tests were performed on collagen/fibronectin matrix samples (8 mm diameter disk, 1.1 mm thick, prepared as described below) using an oscillatory rheometer (Anton-Paar) in parallel-plate geometry. The appropriate amplitude of deformation was determined to be 5% and the plate gap was set between 0.9 and 1.1 mm. Storage and loss moduli (G' and G'', respectively) were measured at 37 °C at frequencies ranging from 0.1–100 s^{-1}. All samples exhibited plateau moduli between 0.2 and 1 s^{-1}.

Human dermal microvascular endothelial cell culture

Adult human dermal microvascular endothelial cells (HDMVEC, Lonza, Walkersville, MD) were grown in Endothelial Growth Medium-2MV (EGM-2MV, 5% serum, Lonza). Media were changed every two days, and cells were kept in a humidified, 5% CO_2 environment at 37 °C. HDMVEC were passaged non-enzymatically using EDTA solution (Gibco, Grand Island, NY). Passages 3–8 were used for each experiment, and the behavior of cells remained the same during these passages. Dry microcarrier dextran beads ($d \approx 170$ μm, Cytodex-3, GE Healthcare) were swollen and hydrated in PBS, rinsed in fresh PBS, and autoclaved. The sterilized solution was allowed to separate in a well plate, and the supernatant was decanted. Microcarrier beads were rinsed twice in EGM-2MV and gradually added to a 10-cm, non-tissue culture plate to homogeneously cover the plate surface with beads. HDMVEC (7×10^6 cells per

 This journal is © The Royal Society of Chemistry 2010

Published on 01 September 2010 on http://pubs.rsc.org | doi:10.1039/C005069E
Downloaded by Stanford University on 29/03/2013 22:44:17.

10-cm plate) were incubated with the beads on a platform shaker inside the incubator for 3–4 hours. After cell adhesion to the beads, the beads were transferred to a fresh 6-well plate and allowed to settle before the supernatant was replaced with 2 ml of fresh serum-free media. In order to estimate the bead concentration, a specified volume of media was placed on a microscope slide and beads were counted using phase contrast microscopy.

Tissue culture inside microfluidic devices

Stock rat tail collagen Type I (BD Biosciences) was mixed with fibronectin (final concentration of 5 μg ml^{-1}, 10% total volumetric mixture) and the media containing microcarrier beads (final concentration of ~20 beads per device) and transformed into the gel phase by the addition of sodium hydroxide (0.5 N stock solution, 0.05% volumetric mixture with stock collagen). Different densities of collagen gel were made by altering the collagen concentration while keeping the final fibronectin, microcarrier bead, and media concentrations uniform. Immediately after mixing, ~20 μl of the solution were injected into the cell culture chamber of the microfluidic device; gelation occurred in 5–10 minutes. Both ends of the cell culture chamber were pin-plugged, and the device was covered with media to avoid gel evaporation. EGM-2MV supplemented with various concentrations of VEGF (VEGF-A isoform VEGF(165), R&D Systems, Minneapolis, MN) was continuously supplied to the source reagent channel, while EGM-2MV with no VEGF was supplied to the sink reagent channel. The injection flow rate was 40 nl min^{-1}. The entire system (microfluidic device, syringe pump, and syringes) was placed in the incubator during the 4 days of cell culture. Syringes were filled with fresh media every day.

Characterization of endothelial cell sprouts and statistical analysis

Individual beads were imaged every 24 h for 2–4 days using phase contrast and fluorescence microscopy. Micrographs were analyzed by hand using ImageJ software (NIH freeware) to measure the number of sprouts per bead, the sprout average thickness, and the sprout initiation angle (ϕ). The average thickness of each sprout was determined by dividing the projected sprout surface area by the length of the sprout centerline. All data are reported as average ± standard deviation. For each condition reported, between three and six independent experiments were performed and ~20 beads per device were imaged in each experiment for a total of 60–120 individual beads per condition. The average number of sprouts per bead was calculated for each individual device. Average and standard deviation of device values were reported in the results. One-tailed, non-paired, Student's *t*-test was used to determine the statistical significance of differences between pairs of conditions.

Cell fluorescent staining

Sprouts within collagen gels were fixed by injecting 4% paraformaldehyde into the source and sink channels and incubating at 4 °C for ~1 h. The samples were washed at least four times by injecting PBS into the source and sink channels. The cells were blocked with 10% normal goat serum in PBST (0.3% Triton X-100 in PBS solution) for ~3 h. Cell nuclei and actin cytoskeleton were stained overnight at 4 °C using DAPI and Alexa Fluor 555-conjugated phalloidin (Invitrogen), respectively. Samples were washed with PBS at least four times and then incubated with PBS at 4 °C for ~12 h prior to imaging. A laser scanning confocal inverted fluorescence microscope (Zeiss) was used to acquire images. All data are reported as average ± standard deviation. For each condition reported, at least $n = 3$ independent experiments were performed. One-tailed, non-paired, Student's *t*-test was used to determine the statistical significance of differences between pairs of conditions.

Results

Microfluidic device development for sprouting angiogenesis

In order to study EC sprouting in response to the combined effects of soluble biochemical concentration gradients and biomechanical matrix properties, adult human dermal microvascular ECs (HDMVECs) were cultured within matrices of varying density inside a microfluidic device (Fig. 1). All matrices included a constant supplement of 5 μg ml^{-1} fibronectin with varying collagen density. Collagen is a main component of ECM and has been used extensively for 3D EC cultures. Several microfluidic devices have been designed to enable the generation of stable biomolecule gradients for a variety of applications.[33–38] The device used here is a slight modification of our previously reported design that includes source and sink channels connected to a cell culture chamber via microcapillaries.[15] By altering the relative VEGF concentrations in the source and sink channels, stable and predictable VEGF concentration profiles are formed (Fig. 2).

To modify the device for 3D cultures and to accommodate the easy injection of cell-coated microcarrier beads and gel matrices, the height of the cell culture chamber was increased from 120 μm in the original device for 2D cultures to 240 μm in the 3D device. Due to the presence of a matrix within the cell culture chamber, flow rates within the sink and source reagent channels were increased from 8 nl min^{-1} in the 2D device to 40 nl min^{-1} for the 3D device without introducing any observable flow in the cell culture chamber. This increased flow rate maintains constant concentrations in the sink and source channels with only single channel inputs as opposed to the dual channel inputs required in the previous device. Since the matrix restricts flow in the cell culture chamber, the widths of the microcapillaries could be increased from 5 to 15 μm and the heights from 4 to 15 μm. This design change enabled more efficient device fabrication and decreased the diffusion time required to achieve a fully developed concentration profile. As the matrices are not subjected to direct fluid flow, they are stable over the four days of the experiment with no observable erosion.

Matrix density mediates EC sprout morphology and initiation rate

Five collagen gel densities (0.3, 0.7, 1.2, 1.9 and 2.7 mg ml^{-1}) were selected to determine the effects of matrix biomechanics on the formation of EC capillary-like sprouts. These selected densities produce gels with plateau storage moduli, G', ranging from 7–700 Pa (Fig. S1†). To first determine the appropriate VEGF concentration range for our studies, sprout formation was initially studied in response to uniform VEGF concentrations

Downloaded by Stanford University on 29/03/2013 22:44:17.
Published on 01 September 2010 on http://pubs.rsc.org | doi:10.1039/C005069E

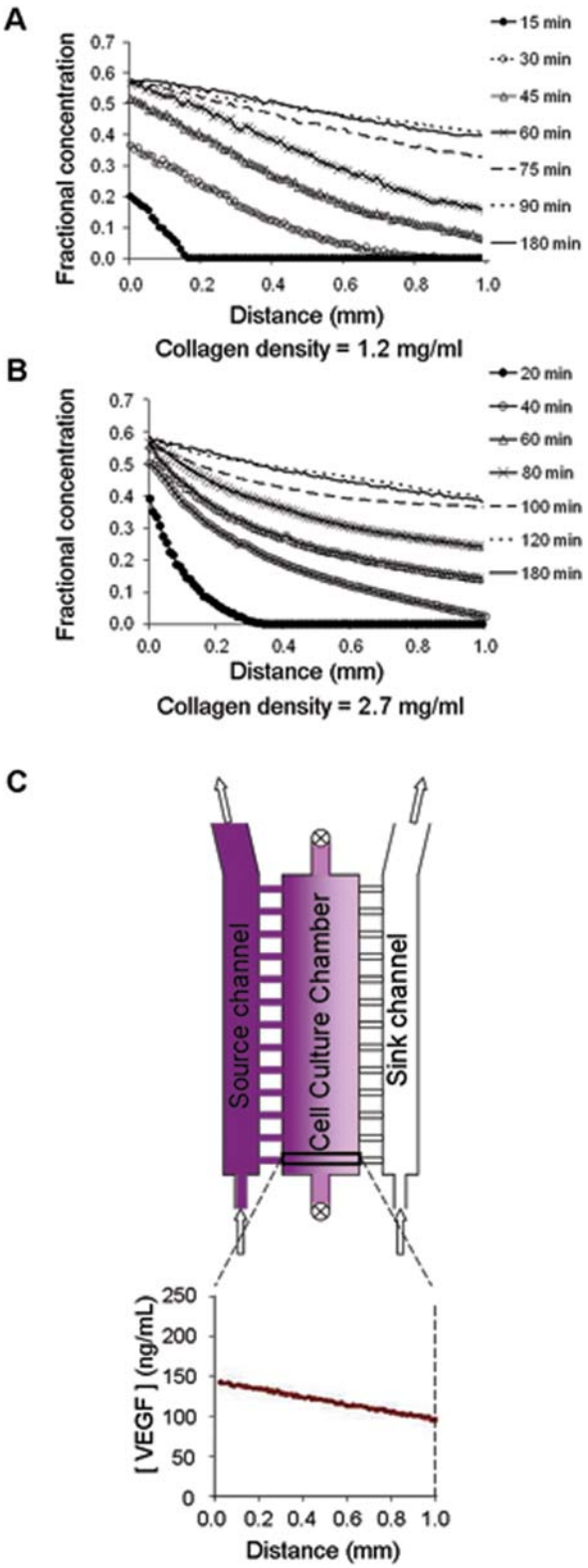

Fig. 2 (A and B) Development of concentration gradient profiles over time. Fractional concentration gradient profile of FITC-labeled dextran (M_w = 20 kDa, similar to VEGF-165) in the microfluidic device. For lower density gels, the gradient more quickly stabilizes to form an equilibrium profile (~90 min for 1.2 mg ml^{-1} collagen compared to 120 min for 2.7 mg ml^{-1}); however, at equilibrium, the concentration profile within all gels is identical. (C) A 2D top-view schematic of the microfluidic device and the quantified equilibrium VEGF profile within the cell culture chamber.

(Fig. S2†). Consistent with other reports that saturating VEGF concentrations of ~100 ng ml^{-1} are effective in sprout formation,[16] we observed increased sprout formation at or above 125 ng ml^{-1}. Based on these data, a VEGF concentration gradient was chosen with a steepness of ~50 ng ml^{-1} mm^{-1} and an average concentration of ~125 ng ml^{-1}. While collagen matrices of varying density displayed altered diffusivities, and hence required a range of 50 to 120 min to reach equilibrium, all matrices had similar final equilibrium VEGF concentration profiles (Fig. 2).

Within this VEGF gradient at low collagen densities (0.3 mg ml^{-1}), ECs quickly migrated into the matrix as single cells without forming cohesive sprout structures (Fig. 3, column A). Short and unstable sprout formation was observed very rarely within this collagen matrix (see third image from the top in Fig. 3, column A). At slightly increased collagen densities (0.7 mg ml^{-1}), tracks of multiple cells began to coordinate their migration to form unstable structures within 24 hours (Fig. 3, column B). Occasionally, these tracks of cells were observed to form preliminary sprout-like structures that commonly were only a single cell in diameter (see third and forth images in Fig. 3, column B). In marked contrast, stable sprouts were formed at intermediate collagen densities after two to three days in culture (1.2 mg ml^{-1} and 1.9 mg ml^{-1}; Fig. 3, columns C and D). On average, sprouts in the 1.2 mg ml^{-1} density matrix were thinner and longer than sprouts in the 1.9 mg ml^{-1} density matrix. At the highest tested collagen density (2.7 mg ml^{-1}), the cells assembled into clusters that formed thick protrusions on the bead and did not elongate into sprouts significantly (Fig. 3, column E). Quantification of the above observations for multiple independent trials confirmed that the number of sprouts initiated per bead was increased for intermediate collagen densities (1.2 and 1.9 mg ml^{-1}; Fig. 4A) and that sprout thickness increased (Fig. 4B) and sprout length decreased (Fig. 4C) with increasing density. In addition, the time required for new sprouts to assemble was increased with increasing density (Fig. 4D), suggesting that the rate of new sprout formation is limited by the migration speed through the 3D matrix. It has been previously reported that cells in denser matrices migrate at slower speeds, presumably due to the requirement of additional proteolytic activity to remodel the surrounding matrix as further described in the Discussion.[7]

Matrix rigidity mediates sprout polarization within stable VEGF gradients

VEGF gradients were previously reported to polarize sprout *elongation* parallel to the concentration profile;[16] however, these studies did not report on the potential polarization at the point of sprout *initiation* and did not examine the effects of matrix density. To evaluate the sprout initiation point, the beads were divided into two hemispheres facing higher (ϕ = 0–180°) or lower (ϕ = 180–360°) VEGF concentrations (Fig. 5A). By comparing the number of sprouts initiated on each side of the bead, we obtained a quantitative measure for the bead polarity (Fig. 5B). At higher collagen densities (1.9 and 2.7 mg ml^{-1}), significant polarization was observed ($p < 0.01$). Less pronounced bead

 This journal is © The Royal Society of Chemistry 2010

Published on 01 September 2010 on http://pubs.rsc.org | doi:10.1039/C005069E
Downloaded by Stanford University on 29/03/2013 22:44:17.

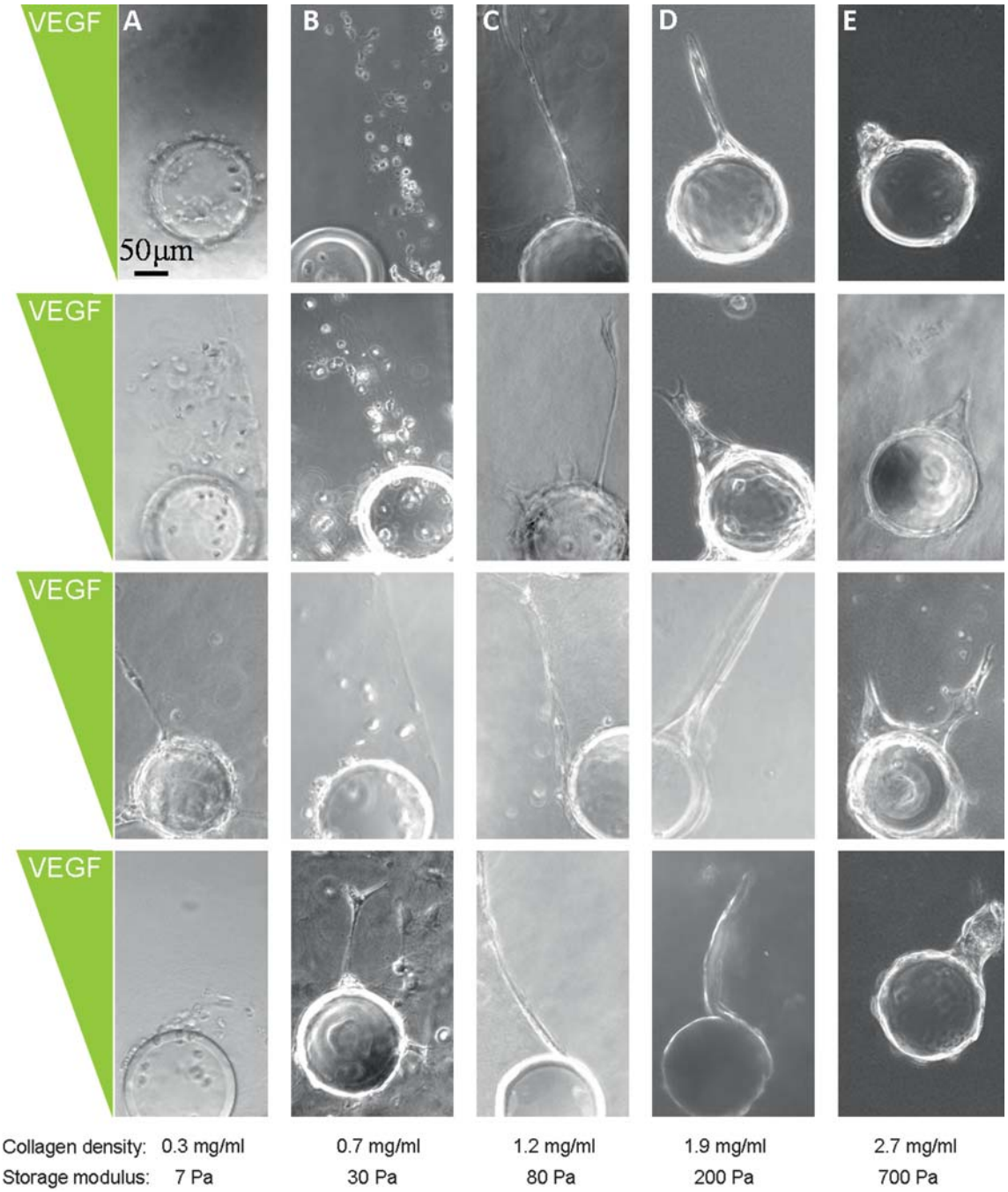

Fig. 3 Sprouting morphogenesis at varying matrix densities. Columns A–E: representative phase contrast images of sprout morphology. (A and B) At low collagen densities (0.3 and 0.7 mg mL^{-1}) single cells migrate into the gel without forming a significant number of stable sprouts. (C and D) At intermediate collagen densities (1.2 and 1.9 mg mL^{-1}) multiple cells coordinate their migration to form extended stable sprouts. (E) At a high collagen density (2.7 mg mL^{-1}) cells form thick protrusions that do not elongate into the matrix significantly.

polarization was observed for the more compliant matrix (1.2 mg ml^{-1}, $p < 0.05$). For the most compliant gel (0.7 mg ml^{-1}), no polarization was observed. Together, these results demonstrate that the ability of a VEGF concentration gradient to induce polarization of sprout initiation is mediated by the matrix density. This implies that matrix rigidity mediates cellular response to VEGF signaling, suggesting a complex relationship between biochemical and biomechanical signals in angiogenic sprouting. In support of this interpretation, recent studies have reported that endothelial cells respond to matrix mechanics by altering their VEGF receptor 2 (VEGFR2) expression levels,[2] which may then alter VEGF-induced sprouting.

Lumen formation and local cell density is enhanced in rigid matrices

As angiogenesis progresses, the stalk cells within the multicellular sprouts organize into tubular structures with hollow

Downloaded by Stanford University on 29/03/2013 22:44:17.
Published on 01 September 2010 on http://pubs.rsc.org | doi:10.1039/C005069E

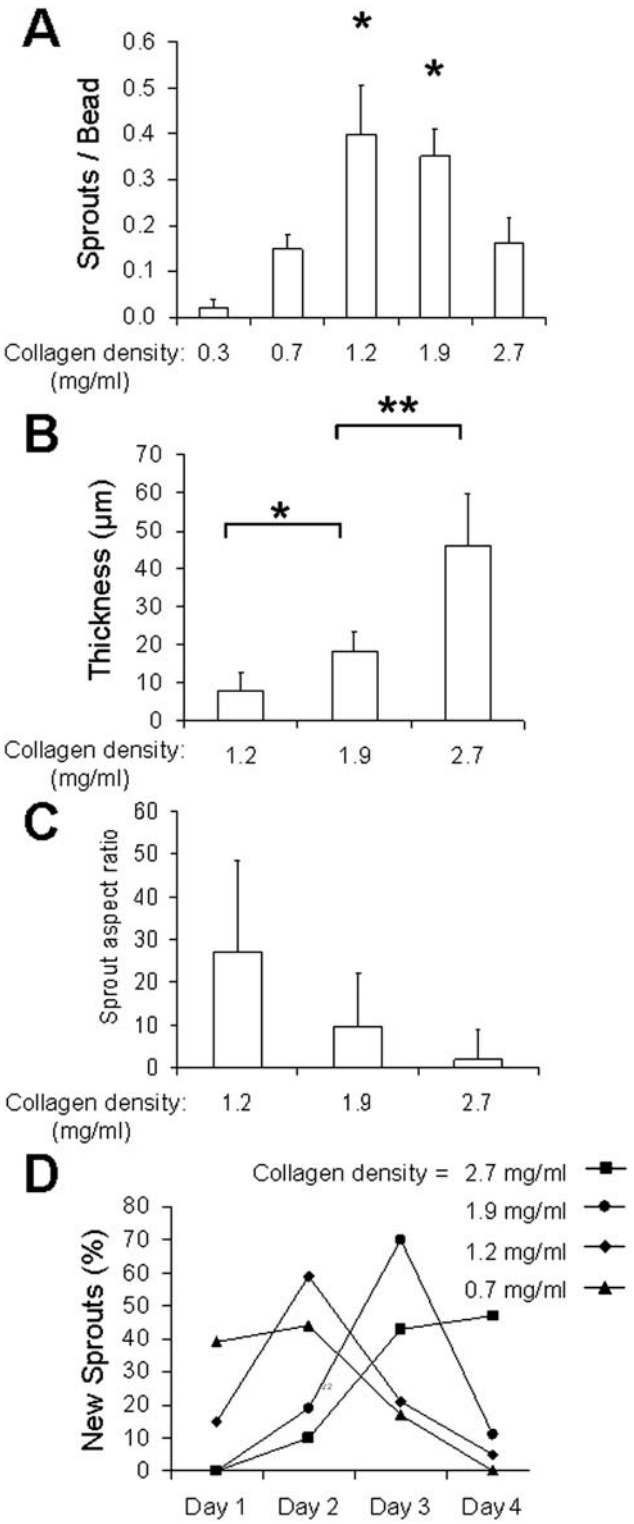

Fig. 4 Sprouting characteristics at varying matrix densities. (A) Total number of sprouts formed per bead. (B) Average sprout thickness. (C) Average aspect ratio (sprout length to width). (D) Number of new sprouts observed at various time points normalized to the total number of observed sprouts. For (A)–(D), $n > 3$ microdevices, each containing ~20 beads, $*p < 0.05$; $**p < 0.01$.

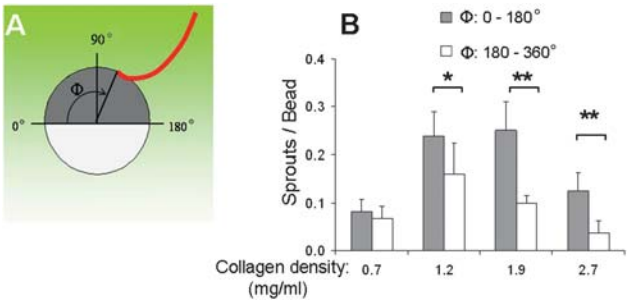

Fig. 5 Polarization of EC sprout initiation point. (A) Schematic of sprout initiation angle relative to VEGF gradient. Bead surface is bisected into two regions: facing towards ($\phi = 0$–$180°$) and away from ($\phi = 180$–$360°$) the gradient. (B) Polarization of sprout initiation point at selected gel densities. Significantly more sprouts are initiated towards higher VEGF concentrations at matrix densities above 1.2 mg ml^{-1}; $*p < 0.05$; $**p < 0.01$.

lumens that can transport blood. This process is hypothesized to be abnormal during tumor-initiated angiogenesis, whereby ECs often fail to form tight luminal junctions resulting in leaky blood vessels.[32] Here we quantified lumen formation within compliant and stiffer matrices in response to a constant, linear VEGF gradient. To investigate the possible role of local cell density in lumen formation, we quantified the number of cells per sprout unit length using a DAPI nuclear stain and confocal microscopy (Fig. 6A–C). In stiffer matrices (density = 1.9 mg ml^{-1}), the number of cells per 10 microns of sprout length was about 50% higher than in more compliant matrices (density = 1.2 mg ml^{-1}). Interestingly, the higher density of cells per sprout length appears to correlate with the ability to form a stable lumen, with an average of three cells per cross-section present in stiffer gels and two cells per cross-section in more compliant gels (Fig. 6A, B, D and E). These results suggest that a minimum number of at least three cells per cross-sectional area may be required to form a lumen with a stable, tube-like geometry.

To quantify lumen formation, we defined the Lumen Formation Index as the length of each sprout section along which a lumen is present normalized to the total length of the sprout, as observed using confocal microscopy. In more compliant gels, sprout cross-sections rarely depict a clearly defined lumen (Fig. 7A). In more rigid matrices, z-stack cross-sections of sprouts taken at ~20 μm intervals clearly depict luminal diameters greater than 10 μm within the sprout sections closest to the sprout initiation point (Fig. 7B, sections 1–3). At cross-sections more distal to the bead (and closer to the tip cell), the luminal diameter decreases and becomes less defined (Fig. 7B, sections 4 and 5). Towards the tip of the sprout, no stable lumen is observed (Fig. 7B, sections 6 and 7). Averaged across three independent trials with $n > 20$ cells per trial, the data demonstrate that stable lumen formation is enhanced within higher density matrices (Fig. 7C).

Discussion

Here we present the development of a microfluidic platform capable of mimicking several key aspects of 3D tissue microenvironments. The ease of fabrication, long-term stability of the concentration gradient within the cell culture chamber, minimized gel contact with fluid flow, and independent control over

 This journal is © The Royal Society of Chemistry 2010

Published on 01 September 2010 on http://pubs.rsc.org | doi:10.1039/C005069E
Downloaded by Stanford University on 29/03/2013 22:44:17.

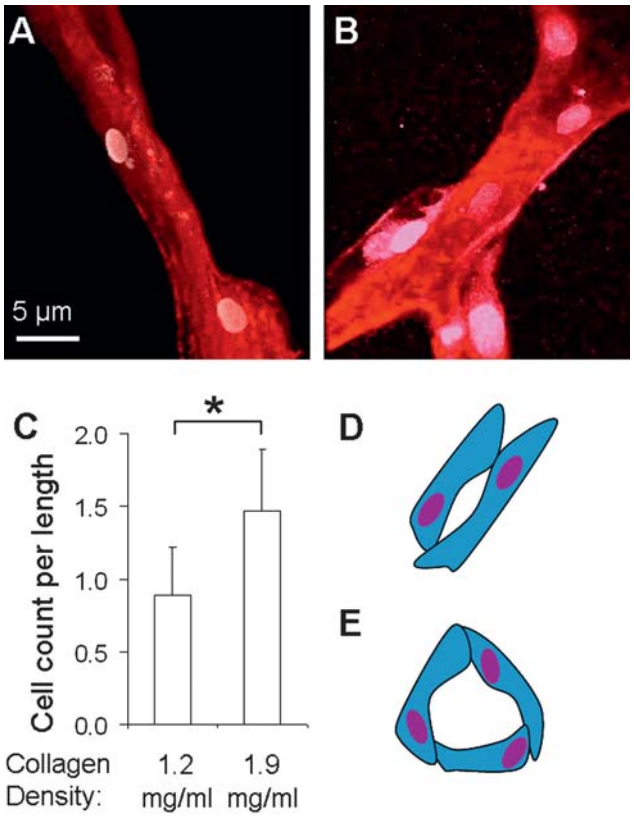

Fig. 6 Cell density within EC sprouts. (A and B) Representative confocal images of multiple ECs (red = phalloidin stain of actin cytoskeleton, white = DAPI stain of nucleus) forming cohesive sprout-like structures in matrices with collagen densities of 1.2 and 1.9 mg ml^{-1}, respectively. (C) Average number of cells per 10 microns of sprout length; *$p < 0.05$. (D and E) Schematic of sprout cross-sections. The average number of cells per cross-sectional area is two within 1.2 mg ml^{-1} matrices and is three within 1.9 mg ml^{-1} matrices, respectively.

biomechanical and soluble biochemical factors are unique features of this microfluidic device compared to previously designed platforms used for 3D cell studies.[27,33–38] Utility of this device was demonstrated by studying the simultaneous roles of matrix density and stable VEGF concentration gradients in regulating EC sprout kinetics, morphology, polarization, and lumen formation.

Recent investigations of sprout formation have revealed that ECs located at various positions along a single sprout undergo specialization into highly migratory tip cells and highly proliferative stalk cells.[39] As the tip cells probe their local environment to sense path-finding cues, they elongate the sprout primarily through their migratory action. In contrast, stalk cells elongate the sprout primarily through their proliferative action resulting in increased numbers of cells. Therefore, the migration rate of the tip cells must be carefully balanced with the proliferation rate of the stalk cells to form a stable EC sprout. Results in this study suggest that the collagen gel density mediates this balance between tip cell migration and stalk cell proliferation. EC migration through 3D protein matrices requires the secretion of protease enzymes that can locally degrade the matrix,[40] the reorganization of the EC cytoskeleton, and the transmission of local traction forces from the cell to the matrix.[41] In response, cell migration through higher density protein matrices is generally much slower than migration through lower density matrices.[7] Therefore, in lower density gels, the ECs may migrate through the matrix more quickly, and new cell proliferation may not be able to occur fast enough to stabilize the potential sprouts (Fig. 3A and B). Results demonstrate that there is an intermediate range of gel stiffness for which the sprout formation is stabilized and optimized ($G' \approx$ 80–200 Pa, Fig. 3C and D). Increasing the matrix density may decrease the migratory capability of the tip cells relative to the proliferation rate of new stalk cells, thereby resulting in later sprout formation (Fig. 4D) with thicker and shorter sprouts (Fig. 4A and B) and more pronounced lumen formation (Fig. 7). Consistent with this hypothesis, at higher matrix densities, cells were unable to migrate into the matrix during the four-day study and formed broad cell clusters of proliferating cells (Fig. 3E).

The relative rates of EC migration and proliferation within various 3D microenvironments may also be the underlying cause for the observed effects on polarized sprout initiation. The VEGF-induced polarization of sprout initiation was significantly greater for beads encapsulated within higher collagen densities (Fig. 5B). This may be because of delayed sprout formation within denser

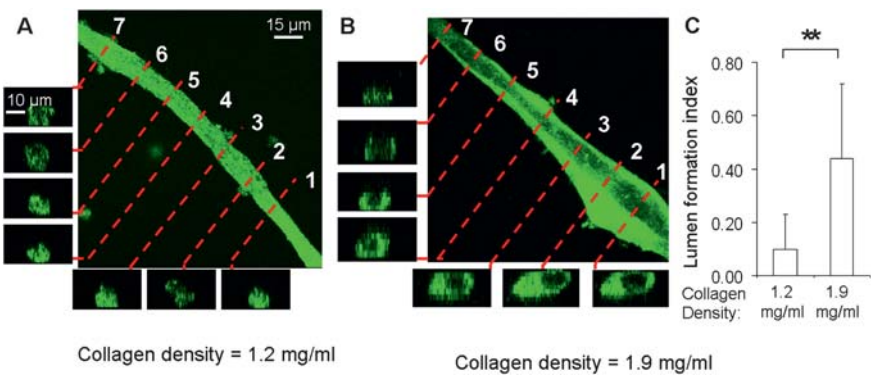

Fig. 7 Lumen formation within EC sprouts. (A and B) Representative confocal images (phalloidin stain of actin cytoskeleton) of sprouts in collagen matrices with densities of 1.2 and 1.9 mg ml^{-1}, respectively. *z*-Stack cross-sections at 20 μm intervals along the length of the sprout show the formation of a hollow lumen structure in the 1.9 mg ml^{-1} matrix. (C) Lumen formation index (*i.e.*, the fractional length of the sprout that has a stable lumen) for matrices of varying density, **$p < 0.01$.

matrices (Fig. 4D), which allows sufficient time for ECs either to migrate on the bead surface to regions of increased VEGF concentration or to proliferate more at those regions. The mechanism of cell migration is thought to be different in 2D versus 3D;[7] therefore it may be possible for cells to migrate in a 2D-manner along the bead surface while they are unable to penetrate into the matrix during the early stages of sprout formation in denser matrices. In contrast, in more compliant matrices, ECs may be able to more easily enter the 3D matrix; therefore, they may be more likely to initiate immature sprouts off of the 2D surface that are misaligned with the VEGF gradient.

These results suggest that only a narrow range of biomechanical environments may be permissible to allow stable sprout formation. Within higher density matrices, the formation of thicker sprouts with more cells per cross-sectional area may result in sprouts with increased ability of lumen formation. Additionally, a decrease in matrix stiffness was observed to correlate with a decrease in stable lumen formation (Fig. 6 and 7).

Taken together, our results demonstrate that matrix density mediates VEGF activity during sprout initiation, sprout elongation, and lumen formation. These findings highlight the importance of considering the biomechanical environment when developing potential new biochemical therapies for pro- and anti-angiogenesis treatments. In addition, this work encourages the further development of future *in vitro* microfluidic platforms that more accurately mimic the *in vivo* environment in a quantifiable and tunable manner. These microfluidic platforms will enable mechanistic studies of sprouting morphogenesis in addition to screening studies of potential pharmacological agents and biomaterial scaffolds within a 3D microenvironment.

Published on 01 September 2010 on http://pubs.rsc.org | doi:10.1039/C005069E
Downloaded by Stanford University on 29/03/2013 22:44:17.

Acknowledgements

The authors thank Ellen Kuhl and Theo Palmer for use of microscopy equipment and Annelise Barron for use of rheometer. Amy Bauer of Los Alamos National Laboratory is thanked for helpful discussions. Funding is acknowledged by the National Academies Keck Futures Initiative CS10, NIH 1DP2 OD006477-01, and NIH 1R21 NS058600-01.

References

1 P. A. Janmey and C. A. McCulloch, *Annu. Rev. Biomed. Eng.*, 2007, **9**, 1–34.
2 A. Mammoto, K. M. Connor, T. Mammoto, C. W. Yung, D. Huh, C. M. Aderman, G. Mostoslavsky, L. E. H. Smith and D. E. Ingber, *Nature*, 2009, **457**, 1103–1157.
3 D. E. Discher, P. Janmey and Y. L. Wang, *Science*, 2005, **310**, 1139–1143.
4 C. M. Nelson and M. J. Bissell, *Annu. Rev. Cell Dev. Biol.*, 2006, **22**, 287–309.
5 A. J. Engler, S. Sen, H. L. Sweeney and D. E. Discher, *Cell*, 2006, **126**, 677–689.
6 M. J. Paszek, N. Zahir, K. R. Johnson, J. N. Lakins, G. I. Rozenberg, A. Gefen, C. A. Reinhart-King, S. S. Margulies, M. Dembo, D. Boettiger, D. A. Hammer and V. M. Weaver, *Cancer Cell*, 2005, **8**, 241–254.
7 M. H. Zaman, L. M. Trapani, A. Siemeski, D. MacKellar, H. Gong, R. D. Kamm, A. Wells, D. A. Lauffenburger and P. Matsudaira, *Proc. Natl. Acad. Sci. U. S. A.*, 2006, **103**, 10889–10894.
8 C. A. Reinhart-King, M. Dembo and D. A. Hammer, *Biophys. J.*, 2005, **89**, 676–689.
9 J. P. Califano and C. A. Reinhart-King, *Cell. Mol. Bioeng.*, 2008, **1**, 122–132.
10 A. L. Sieminski, R. P. Hebbel and K. J. Gooch, *Exp. Cell Res.*, 2004, **297**, 574–584.
11 C. M. Ghajar, X. Chen, J. W. Harris, V. Suresh, C. C. W. Hughes, N. L. Jeon, A. J. Putnam and S. C. George, *Biophys. J.*, 2008, **94**, 1930–1941.
12 W. Risau, *Nature*, 1997, **386**, 671–674.
13 S. Chung, R. Sudo, P. J. Mack, C. R. Wan, V. Vickerman and R. D. Kamm, *Lab Chip*, 2009, **9**, 269–275.
14 P. Vitorino and T. Meyer, *Genes Dev.*, 2008, **22**, 3268–3281.
15 A. Shamloo, N. Ma, M. M. Poo, L. L. Sohn and S. C. Heilshorn, *Lab Chip*, 2008, **8**, 1292–1299.
16 R. R. Chen, E. A. Silva, W. W. Yuen, A. A. Brock, C. Fischbach, A. S. Lin, R. E. Guldberg and D. J. Mooney, *FASEB J.*, 2007, **21**, 3896–3903.
17 V. Vickerman, J. Blundo, S. Chung and R. Kamm, *Lab Chip*, 2008, **8**, 1468–1477.
18 T. M. Keenan, C. H. Hsu and A. Folch, *Appl. Phys. Lett.*, 2006, **89**, 114103.
19 S. Cheng, S. M. Heilman, M. Wasserman, S. Archer, M. L. Shuler and M. Wu, *Lab Chip*, 2007, **7**, 763–769.
20 J. Diao, L. Young, S. Kim, E. A. Fogarty, S. M. Heilman, P. Zhou, M. L. Shuler, M. Wu and M. P. DeLisa, *Lab Chip*, 2006, **6**, 381–388.
21 H. Wu, B. Huang and R. N. Zare, *J. Am. Chem. Soc.*, 2006, **128**, 4194–4195.
22 M. N. Nakatsu, R. C. A. Sainson, J. N. Aoto, K. L. Taylor, M. Aitkenhead, S. Perez-del-Pulgar, P. M. Carpenter and C. C. W. Hughes, *Microvasc. Res.*, 2003, **66**, 102–112.
23 D. Walpita and E. Hay, *Nat. Rev. Mol. Cell Biol.*, 2002, **3**, 137–141.
24 L. G. Griffith and M. A. Swartz, *Nat. Rev. Mol. Cell Biol.*, 2006, **7**, 211–224.
25 K. M. Yamada and E. Cukierman, *Cell*, 2007, **130**, 601–610.
26 N. Yamamura, R. Sudo, M. Ikeda and K. Tanishita, *Tissue Eng.*, 2007, **13**, 1443–1453.
27 S. Chung, R. Sudo, I. K. Zervantonakis, T. Rimchala and R. D. Kamm, *Adv. Mater.*, 2009, **21**, 4863–4867.
28 L. K. W. Chan, *J. Wound Care*, 2009, **18**, 12–14.
29 J. Folkman, *Nat. Med.*, 1995, **1**, 27–30.
30 J. J. Moon and J. L. West, *Curr. Top. Med. Chem.*, 2008, **8**, 300–310.
31 L. Cao and D. J. Mooney, *Adv. Drug Delivery Rev.*, 2007, **59**, 1340–1350.
32 H. Hashizume, P. Baluk, S. Morikawa, J. W. McLean, G. Thurston, S. Roberge, R. K. Jain and D. M. McDonald, *Am. J. Pathol.*, 2000, **156**, 1363–1380.
33 Y. C. Toh, C. Zhang, J. Zhang, Y. M. Khong, S. Chang, V. D. Samper, D. van Noort, D. W. Hutmacher and H. R. Yu, *Lab Chip*, 2007, **7**, 302–309.
34 V. V. Abhyankar, M. W. Toepke, C. L. Cortesio, M. A. Lokuta, A. Huttenlocher and D. J. Beebe, *Lab Chip*, 2008, **8**, 1507–1515.
35 R. Sudo, S. Chung, I. K. Zervantonakis, V. Vickerman, Y. Toshimitsu, L. G. Griffith and R. D. Kamm, *FASEB J.*, 2009, **23**, 2155–2164.
36 A. P. Wong, R. Perez-Castillejos, J. C. Love and G. M. Whitesides, *Biomaterials*, 2008, **29**, 1853–1861.
37 I. Barkefors, S. Le Jan, L. Jakobsson, E. Hejll, G. Carlson, H. Johansson, J. Jarvius, J. W. Park, N. L. Jeon and J. Kreuger, *J. Biol. Chem.*, 2008, **283**, 13905–13912.
38 J. He, Y. Du, J. Villa-Uribe, C. Hwang, D. Li and A. Khademhosseini, *Adv. Funct. Mater.*, 2010, **20**, 131–137.
39 H. Gerhardt, M. Golding, M. Fruttiger, C. Ruhrberg, A. Lundkvist, A. Abramsson, M. Jeltsch, C. Mitchell, K. Alitalo, D. Shima and C. Betsholtz, *J. Cell Biol.*, 2003, **161**, 1163–1177.
40 C. M. Ghajar, S. C. George and A. J. Putnam, *Crit. Rev. Eukaryotic Gene Expression*, 2008, **18**, 251–278.
41 A. Mammoto, J. E. Sero, T. Mammoto and D. E. Ingber, *Methods Enzymol.*, 2008, **443**, 227–259.

 This journal is © The Royal Society of Chemistry 2010